CDF/ANAL/BOTTOM/PUBLIC/10206
Version 1.1
November 2, 2010

# An Updated Measurement of the *CP* Violating Phase $\beta_s^{J/\psi\phi}$ in $B_s^0 \to J/\psi\,\phi$ Decays using 5.2 fb$^{-1}$of Integrated Luminosity

The CDF Collaboration[1]
[1] *www-cdf.fnal.gov*

We present an update of the measurement of the *CP* violation parameter $\beta_s^{J/\psi\phi}$ in flavor-tagged $B_s^0 \to J/\psi\,\phi$ decays using 5.2 fb$^{-1}$ of data collected between February 2002 and June 2009. We find $\sim 6,500$ $B_s^0 \to J/\psi\,\phi$ candidate events in the selected sample, more than doubling the statistics used in the previous, 2.8 fb$^{-1}$ analysis of $\beta_s^{J/\psi\phi}$ released for ICHEP 2008. We report one- and two-dimensional confidence regions in the $\beta_s^{J/\psi\phi}$ and $\beta_s^{J/\psi\phi} - \Delta\Gamma$ planes.We find that the probability of a fluctuation from the standard model expectation to the observed result (*i*.e. frequentist *p*-value) in the $\beta_s^{J/\psi\phi} - \Delta\Gamma$ plane is 44% ($0.8\sigma$), while the *p*-value of $\beta_s^{J/\psi\phi}$ in one-dimension is 31% ($1.0\sigma$). Additionally, we measure the mean $B_s^0$ lifetime $\tau_s$, the width difference of the heavy and light mass eigenstates $\Delta\Gamma$, the transversity amplitudes $|A_0(0)|^2$, $|A_\parallel(0)|^2$, and $|A_\perp(0)|^2$, and the strong phase $\delta_\perp$ assuming that no *CP* violation ($\beta_s^{J/\psi\phi} = 0.0$) is present. We obtain

$$\begin{aligned}
\tau_s &= 458.7 \pm 7.5(\text{stat}) \pm 3.6(\text{syst})\ \mu\text{m}, \\
\Delta\Gamma &= 0.075 \pm 0.035(\text{stat}) \pm 0.01(\text{syst})\ \text{ps}^{-1}, \\
|A_0(0)|^2 &= 0.524 \pm 0.013(\text{stat}) \pm 0.015(\text{syst}), \\
|A_\parallel(0)|^2 &= 0.231 \pm 0.014(\text{stat}) \pm 0.015(\text{syst}), \\
\delta_\perp &= 2.95 \pm 0.64(\text{stat}) \pm 0.07(\text{syst}).
\end{aligned}$$

The obtained results are consistent with previous determinations of these quantities and the measurements of the lifetime, width difference, and transversity amplitudes are now the most precise measurements of these quantities.

## I. INTRODUCTION

We present an update of the measurement of the *CP*-violating phase $\beta_s^{J/\psi\phi}$ in $B_s^0 \to J/\psi\,\phi$ decays, where $J/\psi \to \mu^+\mu^-$ and $\phi \to K^+K^-$. The previous CDF measurements of this quantity observed $1.5\sigma$ and $1.8\sigma$ deviations from the standard model expectation in 1.35 fb$^{-1}$ [1] and 2.8 fb$^{-1}$ [2] of integrated luminosity, respectively. When the latter result is combined with the most recent result from the D0 collaboration [3], the discrepancy with the standard model is $2.1\sigma$. It is worthwhile to note that the more recent CDF result did not fully utilize particle identification information available in data. The present result, which has been updated to 5.2 fb$^{-1}$, is of interest not only because of the dataset is doubled, but also because particle identification is now available and utilized in both selection and tagging.

Since the release of the previous results, considerable interest has fomented concerning a possible non-resonant $K^+K^-$ or $f_0$ contamination in the $\phi$ signal. While the $\phi$ is a vector resonance, the $f_0$ is a pseudo-scalar meson and the non-resonant $K^+K^-$ contribution is in spin 0 state. A significant presence of either contribution in addition to the $\phi$ may lead to biases in the determination of $\beta_s^{J/\psi\phi}$ [4, 5]. In order to address these concerns experimentally, we now include a possible $S$-wave contribution to the signal probability distribution function of the maximum likelihood fit. We have also studied the invariant mass distribution of the $K^+K^-$ as a cross-check of our likelihood fit.

The measurement presented in this note follows closely the techniques and strategy of the previous tagged analyses of $\beta_s^{J/\psi\phi}$ [1, 2]. The reconstructed data is selected via an artificial neural network (ANN) and the determinations of the transversity angles and their efficiencies are identical to the previous measurements. The same-side kaon tagging (SSKT) is now calibrated for the full 5.2 fb$^{-1}$ dataset with an updated $B_s^0$ mixing measurement [6] and the opposite-side flavor tags (OST) are calibrated on $B^+ \to J/\psi\,K^+$ decays separately for $B^+$ and $B^-$. As mentioned above, the likelihood fit now includes an $S$-wave contribution and Feldman-Cousins, coverage-adjusted contours are given in the $\beta_s^{J/\psi\phi} - \Delta\Gamma$ plane for both the tagged and untagged fit.

## II. DATA SELECTION AND RECONSTRUCTION

As in the previous measurements, we use data collected with the di-muon $J/\psi$ trigger [7]. The data sample used was collected between February 2002 and June 2009 and corresponds to an integrated luminosity of 5.2 fb$^{-1}$. Below we define the variables used in the selection and fit to the data. For event selection, we use a loose initial selection to suppress background followed by an artificial neural network (NN), both of which are described in the following sections.

### A. Definition of inputs to selection and fit

In the course of the analysis, a number of quantities are reconstructed from the data. They are used either as inputs to the neural network for selection or as a fit variables. Their definitions are:

- $\chi^2_{\mathbf{r}\phi}(\mathbf{p})$ - The $\chi^2$ of the kinematic fit, including appropriate topology and mass constraints for particle $p$, taking into account only the plane transverse to the proton beam.
- $\mathbf{P}(\chi^2, \mathbf{p})$ - $\chi^2$ probability of the kinematic fit including appropriate topology and mass constraints for particle $p$. This is based on full $\chi^2$ including the z-direction.
- $\mathbf{p_T}(\mathbf{p})$ - Momentum component transverse to the proton beam direction for particle $p$.
- $\mathbf{LL}_\mu(\mathbf{p})$ - Value of likelihood based quantity for muon identification [8].
- $\mathbf{LL_K}(\mathbf{p})$ - Value of likelihood based discriminant for particle identification. It is constructed based on $dE/dx$ and TOF information using latest calibrations. It is calculated using

$$LL_K(p) = \frac{P^K_{\mathrm{d}E/\mathrm{d}x}(p) P^K_{TOF}(p)}{\sum_{j=\pi,K,p} f_j P^j_{\mathrm{d}E/\mathrm{d}x}(p) P^j_{TOF}(p)}, \tag{1}$$

  where $P^i_{dE/dx}$ is probability to observe given $dE/dx$ value under hypothesis $i$ ($\pi$, $K$, $p$), $P^i_{TOF}$ is analogous quantity based on TOF measurement and $f_\pi = 0.7$, $f_K = 0.2$ and $f_p = 0.1$ are the fractions of different particle types in data.

- **ct** - the proper decay time defined as

$$ct = c\frac{\vec{L_{xy}} \cdot \vec{p_T}}{|\vec{p_T}|^2} M, \tag{2}$$

where $\vec{L_{xy}}$ is transverse displacement of the secondary vertex from primary vertex, $\vec{p_T}$ is transverse momentum, and $M$ is world average mass of given particle [9].

- $\sigma_{\mathbf{ct}}$ - the event-by-event uncertainty of proper decay time is obtained from the uncertainty of $\vec{L_{xy}}$, assuming other quantities in equation 2 to have negligible uncertainty.

- $\tilde{\rho} = (\cos\theta, \cos\psi, \phi)$ - angles of the decay calculated in the transversity basis defined in [10]. In the calculation we use four-momenta obtained after the four-track vertex fit. For the masses, we use world average $B_s$ and $J/\psi$ masses and the reconstructed $\phi$ invariant mass.

### B. Initial background suppression

In order to ensure well measured candidates and to reduce size of the data sample we impose several requirements before proceeding to final selection. The applied requirements are:

- Invariant mass of $J/\psi\phi$ pair must lie between 5.1 and 5.6 GeV/$c^2$.
- Transverse momentum of the $B_s^0$ candidate has to be at least 4.0 GeV/$c$.
- The $\chi^2_{r\phi}$ of the kinematic fit where four tracks are constrained to originate from common vertex has to be smaller than 50.
- Each of the four tracks involved is required to have at least 10 axial and 10 stereo hits in the COT and at least 3 axial hits in silicon detector.
- Both kaons are required to have transverse momentum of at least 400 MeV/$c$.
- Minimum transverse momentum of the $\phi$ candidate is 1 GeV/$c$.
- Invariant mass of the muon pair should lie between 3.04 and 3.14 GeV/$c^2$.
- Invariant mass of the kaon pair should be within 1.009 and 1.028 GeV/$c^2$.

### C. Artificial Neural Network

In this subsection we describe the final neural network we use for candidate selection. Compared to the previous version of the analysis [2], we have increased the statistics in the training and removed some of the input variables without a significant loss in selection power.

To construct the neural network, we use the NeuroBayes package [11]. The neural network is trained using simulated events as signal samples and $B_s^0$ invariant mass sideband regions, $m(J/\psi\phi) \in [5.2, 5.3]$ GeV/$c^2 \bigcup \in [5.45, 5.55]$ GeV/$c^2$, as background samples. As a loss function we employ an entropy function. During the training process we do not apply re-weighting of the simulated events. The training sample consists of about $350 \times 10^3$ signal events and about $300 \times 10^3$ background events.

In Table I we list the input variables to the neural network training, the ranking of the inputs, and the significance of the inputs. The rank sorts the variables according to their importance. We show a graphical representation of the correlation matrix between inputs to the neural network and truth information in Fig. 1. Figure 2 shows the distribution of the neural network output for signal and background and the signal purity (fraction of signal events in selected events) as a function of ANN selection. In these plots, the training sample is used to indicate signal and background.

Using simulated experiments we choose a selection value of the NN output variable that maximizes sensitivity to $\beta_s^{J/\psi\phi}$. Amount of signal and background similated is determined from a single Gaussian fit to the invariant mass distribution. The values of the other input parameters are fixed to the result of our previous measurement on 2.8 $fb^{-1}$ of data [2]. Optimization plots for several true values of the $\beta_s$ are shown in Fig. 3. We choose to apply a cut on the NN output variable at 0.2 for the $B_s^0$ signal, which provides the smallest statistical uncertainty on $\beta_s^{J/\psi\phi}$ while still giving a reasonable signal to background ratio. With this selection we find $6,504 \pm 85$ $B_s^0$ signal candidates.

| Variable | Rank | Index |
|---|---|---|
| $p_T(\phi)$ | 1 | 5 |
| $LL_K(K_2)$ | 2 | 11 |
| $LL_K(K_1)$ | 3 | 10 |
| $LL_\mu(\mu^+)$ | 4 | 9 |
| $\chi^2_{r\phi}(B^0_s)$ | 5 | 2 |
| $p_T(B^0_s)$ | 6 | 3 |
| $LL_\mu(\mu^-)$ | 7 | 8 |
| $P(\chi^2, B^0_s)$ | 8 | 4 |
| $P(\chi^2, \phi)$ | 9 | 6 |
| $P(\chi^2, J/\psi)$ | 10 | 7 |

TABLE I: Inputs to the neural network for $B^0_s \to J/\psi\,\phi$ candidate selection. The rank refers to the importance of a given variable in the NN and index numbers inputs for correlation matrix in Fig. 1.

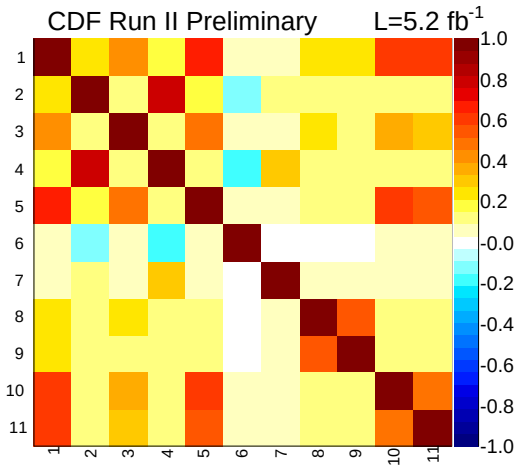


FIG. 1: Graphical representation of the correlation matrix of inputs to the neural network and truth. First row/column represents truth (signal or background) while rest shows different inputs. The Numbers on the x and y axis correspond to the column index in Table I.

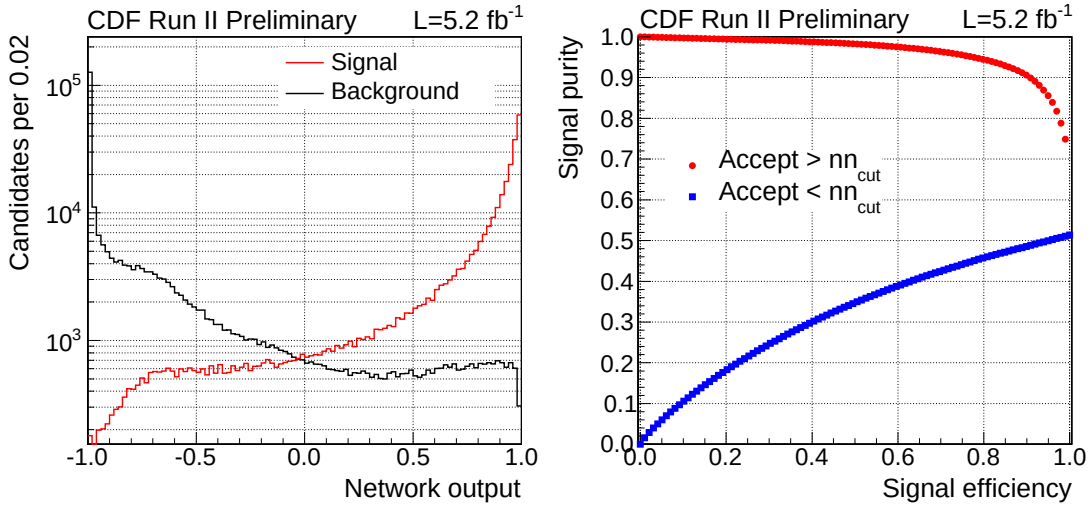


FIG. 2: Distribution of the neural network output for signal (red) and background (black) on training sample (left). Signal purity as a function of neural network output (right).

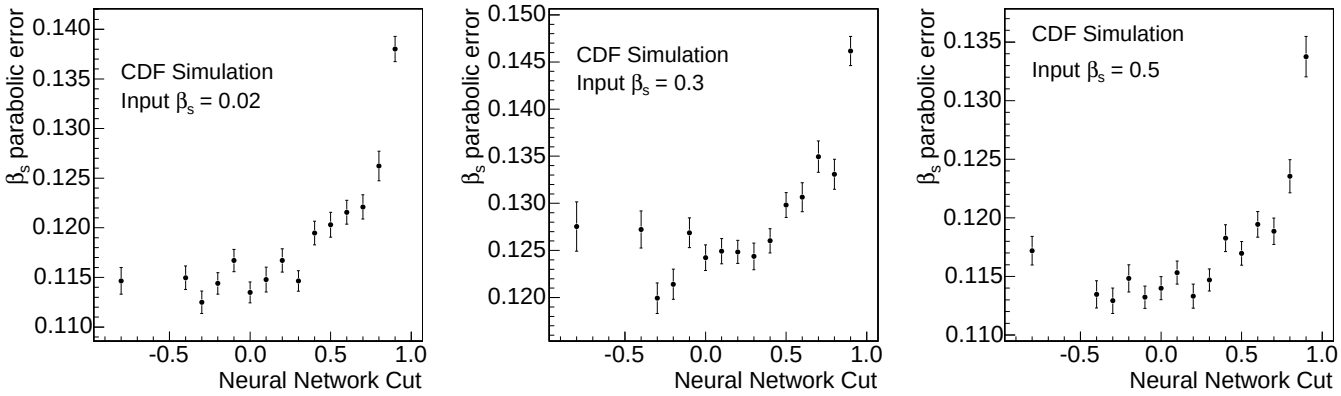


FIG. 3: Expected variance of $\beta_s$ as a function of the minimal requirement on the neural network output for $\beta_s^{J/\psi\phi} = 0.02$ (left), $\beta_s^{J/\psi\phi} = 0.30$ (center), and $\beta_s^{J/\psi\phi} = 0.50$ (right).

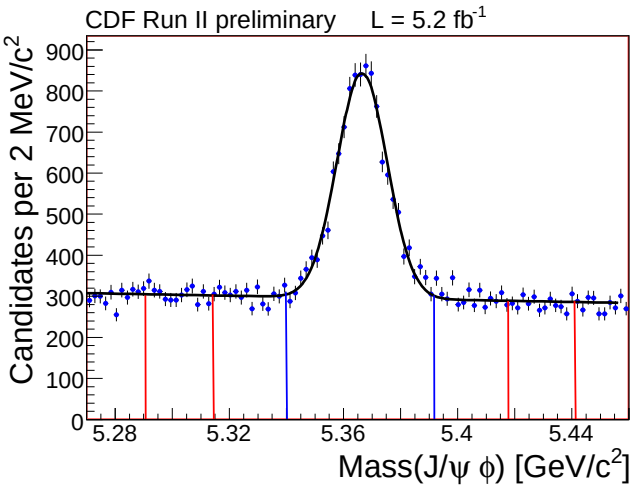


FIG. 4: Invariant mass distributions of $\mu^+\mu^- K^+ K^-$. We find $6,504 \pm 85$ $B_s^0 \to J/\psi\,\phi$ events.

## III. TRANSVERSITY ANGLES

As in the previous untagged and tagged measurements of $\beta_s^{J/\psi\phi}$, this measurement makes use of the transversity angles $\vec{\rho} = (\cos\theta_T, \phi_T, \cos\psi)$ defined in [10], in order to separate the *CP*-even and *CP*-odd components of the $J/\psi\,\phi$ final state. In addition to the straight-forward theoretical prediction for the behavior of the signal, we must take into account the detector effects on the predicted distribution of the transversity angles and we must model the transversity angle distributions of the background. Realistic $B_s^0 \to J/\psi\,\phi$ Monte Carlo, generated according to a phase space decay model, is used to determine the detector sculpting of the angles due to the non-hermeticity of the CDF II detector. The three-dimensional distribution of the angles are fit with expansions of the Legendre polynomials and spherical harmonics, as has been done in the previous measurements [1, 2], to describe the efficiencies in the transversity angles. These efficiencies are then applied to the signal probability distribution function (PDF) in the maximum likelihood fit. The background transversity angles, determined from the $B_s^0$ mass sidebands, are fit with an empirical model that is found to describe the data. As a cross-check, the angular efficiencies determined from Monte Carlo simulation are shown overlaid with the transversity angle distributions from the $B_s^0$ mass sidebands in Fig. 5. The good agreement between the two indicate that the sidebands are consistent with combinatorial background having flat angular distrubutions before detector acceptance effects.

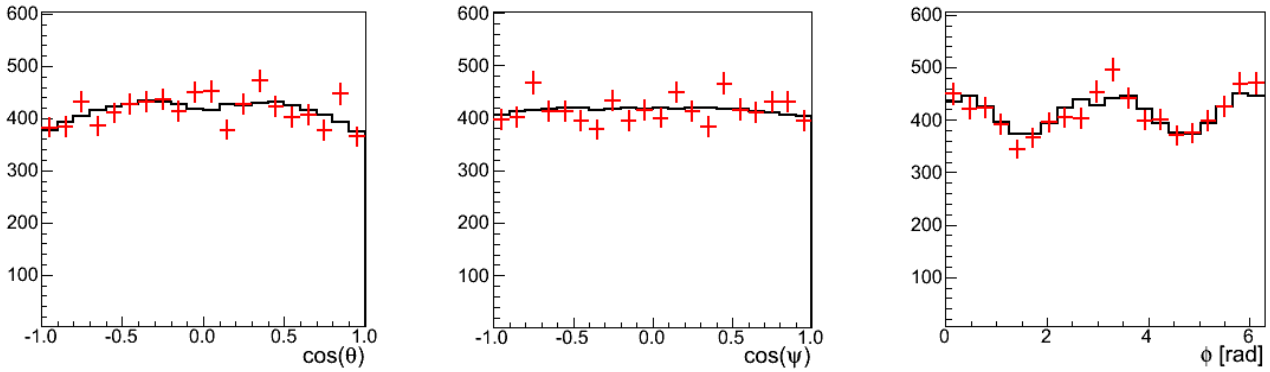


FIG. 5: Comparison of angular efficiencies determined from Monte Carlo simulation (black histogram) and transversity angle distributions obtained from the $B_s^0$ mass sidebands (red points with error bars).

## IV. FLAVOR TAGGING

In this measurement, we use flavor tagging to distinguish the flavor of the $B_s^0$ at production (*i.e.* whether a $B_s^0$ or $\bar{B}_s^0$ was produced) in order to maximize our sensitivity to the *CP*-violating phase $\beta_s^{J/\psi\phi}$. Flavor tagging at CDF takes advantage of the fact that $b$ quarks are produced in quark-antiquark pairs at the Tevatron. Consequently, we can determine information about the flavor of the $B_s^0$ at production by looking at tracks associated with the hadronization of the $b/\bar{b}$ quark that produced the $\bar{B}_s^0/B_s^0$ we observe (called same-side tags or SST), or by looking at the decay products of $B$ hadrons produced by the other $\bar{b}/b$ quark in the event (called opposite-side tags or OST.)

The tagging algorithms output a tag decision indicating whether the meson was $B_s^0$ or $\bar{B}$ at the time of production, as well as a dilution $\mathcal{D}$. The dilution is related to the tagging purity $\mathcal{P}$. $\mathcal{P}$ is the number of correct tags divided by the total tags and is related to $\mathcal{D}$ by $\mathcal{P} = \frac{1+\mathcal{D}}{2}$.

### A. Opposite-side Flavor Tagging

Different tagging algorithms are used to tag the flavor of the opposite-side $b$ quark, depending on whether the opposite side decay products are electrons (soft electron tagger), muons (soft muon tagger), or jets (jet charge tagger). We use an ANN combination of the OST for more optimal tagging power.

The opposite side taggers are calibrated on data from an inclusive sample of semileptonic $B$ decays collected with the $\ell$+SVT trigger [12], while this analysis uses data from the di-muon trigger. Thus, it is necessary to verify that the predicted dilution is not sample dependent, and that the measured dilution on di-muon data matches the predicted dilution from calibration on the $\ell$+SVT data, which are determined from a dataset with a higher $p_T$ spectrum than the data used in this measurement.

Since the dilution for opposite-side tags can be measured directly in a sample of $B^+$ hadrons, we compare the measured dilution in $B^+ \to J/\psi\, K^+$ data as a function of the predicted dilution, which is included event-per-event in the likelihood fit. Dilution is calculated as $D = (C-W)/(C+W)$ where $C(W)$ is the number of correctly (incorrectly) tagged events. Distributions of measured vs. predicted dilutions in $B^+$ can be seen in Fig. 6 for $B^+ \to J/\psi\, K^+$ and $B^- \to J/\psi\, K^-$ events. Using these distributions, we obtain a dilution scale factor of $0.93 \pm 0.09$ for $S_{\mathcal{D}}^+$ and $1.12 \pm 0.10$ for $S_{\mathcal{D}}^-$. We measure a tagging efficiency of $94.3 \pm 0.3\%$ and an average predicted dilution on signal of $0.110 \pm 0.002$.

### B. Same-side Flavor Tagging

The same side kaon tagger (SSKT) uses kaons produced in association with the $B_s^0$ meson that we reconstruct [13]. The $B_s^0$ meson and kaon each contain a strange quark that comes from an $s\bar{s}$ pair. Therefore, a $K^+$ will tag a $B_s^0$ meson, while a $K^-$ tags a $\bar{B}_s^0$ meson. The same side kaon tagging algorithm has not changed from the original $B_s^0$ mixing measurement [14]. The tagger has been calibrated using the most recent measurement of $B_s^0$ mixing [6], which has been made on 5.2 fb$^{-1}$ of $B_s^0 \to D_s^-\pi^+(\pi^-\pi^+)$ data.

As the $B_s^0$ mixing calibration of the SSKT is still statistics limited, we use a single scale factor for the entire data set

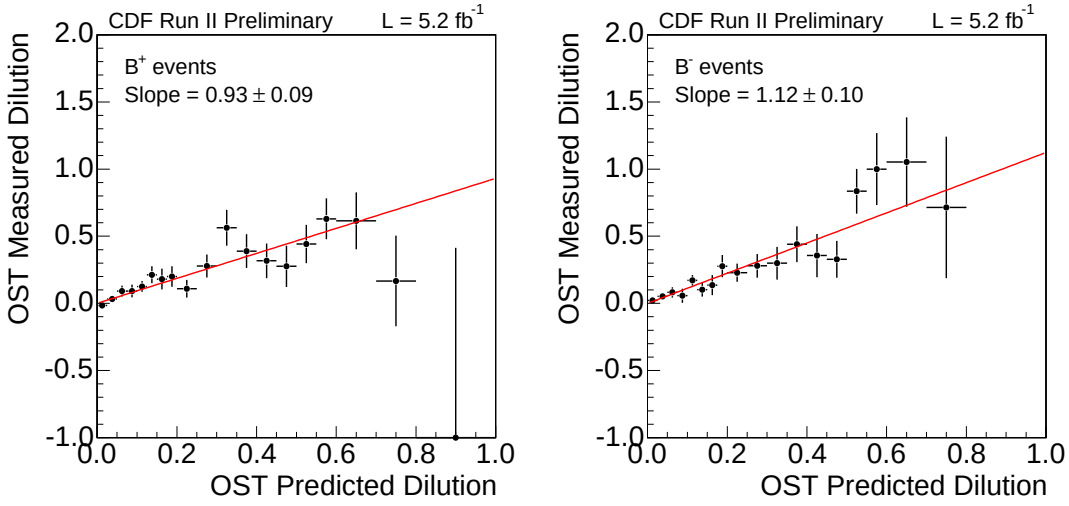


FIG. 6: Comparison of measured dilution as a function of predicted dilution in $B^+ \to J/\psi\, K^+$ data (left) and $B^- \to J/\psi\, K^-$ data (right).

for the same side kaon tagger: $S_{\mathcal{D}} = 0.94 \pm 0.15$ (stat) $\pm 0.13$ (syst). We measure a tagging efficiency of $52.2 \pm 0.7\%$, and an average predicted dilution on signal of $0.275 \pm 0.003$.

## V. UN-BINNED MAXIMUM LIKELIHOOD FIT

The un-binned maximum likelihood fit is similar to that used previously [1], although we have now added an $S$-wave component to the fit that allows for possible contamination of the $\phi \to K^+K^-$ from $f^0 \to K^+K^-(\pi^+\pi^-)$ decays or a non-resonant $K^+K^-$ contribution [4, 5].

The likelihood fit is used to extract the parameters of interest, $\beta_s^{J/\psi\phi}$ and $\Delta\Gamma$, plus additional parameters (referred to as "nuisance parameters") that include, but are not limited to, the signal fraction $f_s$ and mass of the $B_s^0$, the mean $B_s^0$ width $\Gamma \equiv (\Gamma_L + \Gamma_H)/2 \equiv 1/\tau_s$ and background lifetime parameters, the mixing frequency $\Delta m_s$ and flavor-tagging efficiencies and scale factors, the magnitudes of the polarization amplitudes $|A_0|^2$, $|A_\parallel|^2$, and $|A_\perp|^2$ and angular background parameters, and the strong phases $\delta_\parallel \equiv \arg(A_0^* A_\parallel)$ and $\delta_\perp \equiv \arg(A_0^* A_\perp)$. The inputs to the fit include the reconstructed $B_s^0$ candidate mass $m$ and its uncertainty $\sigma_m$, the $B_s^0$ candidate proper decay time $t$ and its uncertainty $\sigma_t$, the transversity angles $\vec{\rho} = \{\cos\theta_T, \phi_T, \cos\psi_T\}$, and tag information $\mathcal{D}$ and $\xi$, where $\mathcal{D}$ is the event-specific dilution and $\xi = \{-1, 0, +1\}$ is the tag decision, in which $+1$ corresponds to a candidate tagged as $B_s^0$, $-1$ to a $\bar{B}_s^0$, and 0 to an untagged candidate.

We have incorporated the $S$-wave component into our fit functions to assess the fraction of events in our data sample which come from $B_s^0 \to J/\psi K^+K^-$ or $B_s^0 \to J/\psi f^0$. As the $f^0$ is a wide resonance, of which only the end of the upper tail lies withing the signal $\phi$ meson mass range, we treat both the non-resonant$KK$ and $f^0$ as being flat in invariant $KK$ mass.

Although the measured effect is small, for a more complete result we have made the $S$-wave fit the default, and all results included in this note are from the fit including $S$-wave $KK$ component unless otherwise stated.

The single-event likelihood is described in terms of signal ($P_s$) and background ($P_b$) probability distribution functions (PDFs) as

$$\begin{aligned} &f_s P_s(m|\sigma_m) P_s(t, \vec{\rho}, \vec{\xi}|\vec{S}_{\mathcal{D}}, \vec{\mathcal{D}}, \sigma_t) P_s(\sigma_t) P_s(\mathcal{D}) \\ &+(1 - f_s) P_b(m) P_b(t|\sigma_t) P_b(\vec{\rho}) P_b(\sigma_t) P_b(\vec{\mathcal{D}}). \end{aligned} \tag{3}$$

The signal mass PDF $P_s(m|\sigma_m)$ is parameterized as a single Gaussian with a standard deviation determined separately for each candidate, while the background mass PDF, $P_b(m)$, is parameterized as a first order polynomial. The distributions of the decay time uncertainty and the event-specific dilution are observed to be different in signal and background, so we include their PDFs explicitly in the likelihood. The signal PDFs $P_s(\sigma_t)$ and $P_s(\vec{\mathcal{D}})$ are determined from sideband-subtracted data distributions, while the background PDFs $P_b(\sigma_t)$ and $P_b(\vec{\mathcal{D}})$ are determined from the $J/\psi\phi$ invariant mass sidebands. The PDFs of the decay time uncertainties, $P_s(\sigma_t)$ and $P_b(\sigma_t)$, are described with

a sum of Gamma function distributions, while the dilution PDFs $P_s(\vec{\mathcal{D}})$ and $P_b(\vec{\mathcal{D}})$ are included as histograms that have been extracted from data.

As discussed in Section IV, we now use separate OST scale factors for positive and negative tags. This slightly modifies the expressions for our decay time signal PDF $P_s(t,\vec{\rho},\vec{\xi}|\vec{\mathcal{D}})$, which is expanded in terms of probability for $B_s^0$ ($P(t,\vec{\rho})$) and $\bar{B}_s^0$ ($\bar{P}(t,\vec{\rho})$),

$$P_s(t,\vec{\rho},\vec{\xi}|\vec{\mathcal{D}}) = \left(\frac{1+\xi_1 S^+_{\mathcal{D},1}\mathcal{D}_1}{1+|\xi_1|}\times\frac{1+\xi_2 S_{\mathcal{D},2}\mathcal{D}_2}{1+|\xi_s|}\right)P(t,\vec{\rho}) + \left(\frac{1-\xi_1 S^-_{\mathcal{D},1}\mathcal{D}_1}{1+|\xi_1|}\times\frac{1-\xi_2 S_{\mathcal{D},2}\mathcal{D}_2}{1+|\xi_2|}\right)\bar{P}(t,\vec{\rho}). \tag{4}$$

where $\{\xi_1,\mathcal{D}_1,S^{\pm}_{\mathcal{D},1}\}$ correspond to the tag decision, predicted dilution, and dilution scale factors of the OST and $\{\xi_2,\mathcal{D}_2,S_{\mathcal{D},2}\}$ correspond to the tag decision, predicted dilution, and scale factor of the SSKT.

In order to determine the time component, we consider the time and angular amplitudes for the $P$-wave and $S$-wave separately. We begin with the probability density for a $P$-wave $B_s^0$ or a $\bar{B}_s^0$ meson decay, which is given by

$$P(\theta,\psi,\phi,t) = \frac{9}{16\pi}(|\mathbf{A}_+\times\hat{n}|^2|f_+(t)|^2 + |\mathbf{A}_-\times\hat{n}|^2|f_-(t)|^2 + 2Re((\mathbf{A}_+\times\hat{n})\cdot(\mathbf{A}_-^*\times\hat{n}))\cdot f_+(t)\cdot f_-^*(t)) \tag{5}$$

and

$$\bar{P}(\theta,\psi,\phi,t) = \frac{9}{16\pi}(|\mathbf{A}_+\times\hat{n}|^2|\bar{f}_+(t)|^2 + |\mathbf{A}_-\times\hat{n}|^2|\bar{f}_-(t)|^2 + 2Re((\mathbf{A}_+\times\hat{n})\cdot(\mathbf{A}_-^*\times\hat{n}))\cdot \bar{f}_+(t)\cdot \bar{f}_-^*(t)), \tag{6}$$

where the unit vector is defined as

$$\hat{n} = (\sin\theta\cos\phi, \sin\theta\sin\phi, \cos\theta), \tag{7}$$

and the angular amplitudes are defined as

$$\mathbf{A}_+ = (A_0\cos\psi, -\frac{A_{||}\sin\psi}{\sqrt{2}}, 0), \tag{8}$$

$$\mathbf{A}_- = (0, 0, i\frac{A_\perp\sin\psi}{\sqrt{2}}), \tag{9}$$

The time-dependent terms $f_+(t)$ and $f_-(t)$ appear in combination as

$$|\bar{f}_\pm(t)|^2 = \frac{1}{2}\frac{(1\pm\cos 2\beta_s^{J/\psi\phi})e^{-\Gamma_L t} + (1\mp\cos 2\beta_s^{J/\psi\phi})e^{-\Gamma_H t} \pm 2\sin 2\beta_s^{J/\psi\phi}e^{-\Gamma t}\sin\Delta m_s t}{\tau_L(1\pm\cos 2\beta_s^{J/\psi\phi}) + \tau_H(1\mp\cos 2\beta_s^{J/\psi\phi})} \tag{10}$$

$$|f_\pm(t)|^2 = \frac{1}{2}\frac{(1\pm\cos 2\beta_s^{J/\psi\phi})e^{-\Gamma_L t} + (1\mp\cos 2\beta_s^{J/\psi\phi})e^{-\Gamma_H t} \mp 2\sin 2\beta_s^{J/\psi\phi}e^{-\Gamma t}\sin\Delta m_s t}{\tau_L(1\pm\cos 2\beta_s^{J/\psi\phi}) + \tau_H(1\mp\cos 2\beta_s^{J/\psi\phi})} \tag{11}$$

$$\bar{f}_+(t)\bar{f}_-^*(t) = \frac{-e^{-\Gamma t}\cos\Delta m_s t - i\cos 2\beta_s^{J/\psi\phi}e^{-\Gamma t}\sin\Delta m_s t + i\sin 2\beta_s^{J/\psi\phi}(e^{-\Gamma_L t} - e^{-\Gamma_H t})/2}{\sqrt{[(\tau_L-\tau_H)\sin 2\beta_s^{J/\psi\phi}]^2 + 4\tau_L\tau_H}} \tag{12}$$

$$f_+(t)f_-^*(t) = \frac{e^{-\Gamma t}\cos\Delta m_s t + i\cos 2\beta_s^{J/\psi\phi}e^{-\Gamma t}\sin\Delta m_s t + i\sin 2\beta_s^{J/\psi\phi}(e^{-\Gamma_L t} - e^{-\Gamma_H t})/2}{\sqrt{[(\tau_L-\tau_H)\sin 2\beta_s^{J/\psi\phi}]^2 + 4\tau_L\tau_H}}. \tag{13}$$

Two modifications are made to make the probabilities realistic to our measurement in the CDF detector environment. First, the exponential and sin functions in the likelihood are replaced with smeared exponential and smeared sin functions to reflect our imperfect lifetime resolution. Secondly, the likelihood is multiplied with a function for the detector efficiency. Hence, $P$ and $\bar{P}$ are transformed to

$$P'(\psi,\theta,\phi,t) = \frac{1}{N}P(\psi,\theta,\phi,t)\epsilon(\psi,\theta,\phi) \tag{14}$$

and

$$\bar{P}'(\psi,\theta,\phi,t) = \frac{1}{N}\bar{P}(\psi,\theta,\phi,t)\epsilon(\psi,\theta,\phi), \tag{15}$$

where $N$ is the normalization, and $\epsilon(\psi,\theta,\phi)$ is the detector efficiency.

For the $S$-wave component, we begin with a normalized probability density

$$\begin{aligned} Q_B(\theta,\phi,\psi,t) &= \frac{3}{16\pi}|\mathbf{B}(t)\times\hat{n}|^2 \\ Q_{\bar{B}}(\theta,\phi,\psi,t) &= \frac{3}{16\pi}|\bar{\mathbf{B}}(t)\times\hat{n}|^2, \end{aligned} \tag{16}$$

where

$$\begin{aligned} \mathbf{B}(t) &= (\mathcal{B}(t),0,0) \\ \bar{\mathbf{B}}(t) &= (\bar{\mathcal{B}}(t),0,0) \end{aligned} \tag{17}$$

and

$$\begin{aligned} \mathcal{B}(t) &= \frac{e^{-imt}e^{-\Gamma t/2}}{\sqrt{\tau_H+\tau_L-\cos 2\beta_s\,(\tau_L-\tau_H)}}\left[E_+(t)-e^{2i\beta_s}E_-(t)\right], \\ \bar{\mathcal{B}}(t) &= \frac{e^{-imt}e^{-\Gamma t/2}}{\sqrt{\tau_H+\tau_L-\cos 2\beta_s\,(\tau_L-\tau_H)}}\left[-E_+(t)+e^{-2i\beta_s}E_-(t)\right]. \end{aligned} \tag{18}$$

The functions $E_+(t)$ and $E_-(t)$ are given by

$$E_\pm(t) \equiv \frac{1}{2}\left[e^{+\left(\frac{-\Delta\Gamma}{4}+i\frac{\Delta m}{2}\right)t} \pm \left[e^{-\left(\frac{-\Delta\Gamma}{4}+i\frac{\Delta m}{2}\right)t}\right]\right]. \tag{19}$$

The equivalent of Eqns. 5 and 6 for the $S$-wave differential rate are

$$\begin{aligned} Q_B(\theta,\psi,\phi,t) &= \frac{3}{16\pi}|\mathbf{B}(t)\times\hat{n}|^2 \\ &= \frac{3}{16\pi}|\mathbf{B}\times\hat{n}|^2|f_-(t)|^2. \end{aligned} \tag{20}$$

and

$$\begin{aligned} Q_{\bar{B}}(\theta,\psi,\phi,t) &= \frac{3}{16\pi}|\bar{\mathbf{B}}(t)\times\hat{n}|^2 \\ &= \frac{3}{16\pi}|\mathbf{B}\times\hat{n}|^2|\bar{f}_-(t)|^2. \end{aligned} \tag{21}$$

In this measurement, we select events whose reconstructed $\phi$ mass $\mu$ lies within a window $\mu_{lo} < \mu < \mu_{hi}$. The normalized probability in this case is

$$\begin{aligned} P(\theta,\phi,\psi,t,\mu) &= \frac{9}{16\pi}\left|\left[\sqrt{1-F_s}g(\mu)\mathbf{A}(t)+e^{i\delta_s}\sqrt{F_s}\frac{h(\mu)}{\sqrt{3}}\mathbf{B}(t)\right]\times\hat{n}\right|^2 \\ \bar{P}(\theta,\phi,\psi,t,\mu) &= \frac{9}{16\pi}\left|\left[\sqrt{1-F_s}g(\mu)\bar{\mathbf{A}}(t)+e^{i\delta_s}\sqrt{F_s}\frac{h(\mu)}{\sqrt{3}}\bar{\mathbf{B}}(t)\right]\times\hat{n}\right|^2, \end{aligned} \tag{22}$$

where $F_s$ is the $S$-wave fraction, $\mu_\phi$ is the $\phi$ mass (1.019 GeV/$c^2$), $\Gamma_\phi$ is the $\phi$ width (4.26 MeV/$c^2$), and $\delta_s$ is the phase of the $S$-wave component relative to the $P$-wave component. $g(\mu)$ is the asymmetric relativistic Breit-Wigner

$\phi$ meson mass propagator, $h(\mu) = \frac{1}{\sqrt{\Delta\mu}}$ is a constant function describing the $f^0$ or non-resonant $K^+K^-$ in the mass window $[1.009, 1.028]$ GeV/$c^2$.

We model the decay time background PDF $P_b(t|\sigma_t)$ with a delta function at $t = 0$, one and two exponentials with negative slope for $t < 0$ and $t > 0$, respectively, all of which are convolved with a two Gaussian resolution function. The background angular PDFs are factorized, $P_b(\vec{\rho}) = P_b(\cos\theta_T)P_b(\varphi_T)P_b(\cos\psi_T)$, and are obtained using $B_s^0$ mass sidebands events.

The signal and sideband region $ct$ fit projections are shown in Fig. 7. Angular fit projections for signal and background are shown in Fig. 8.

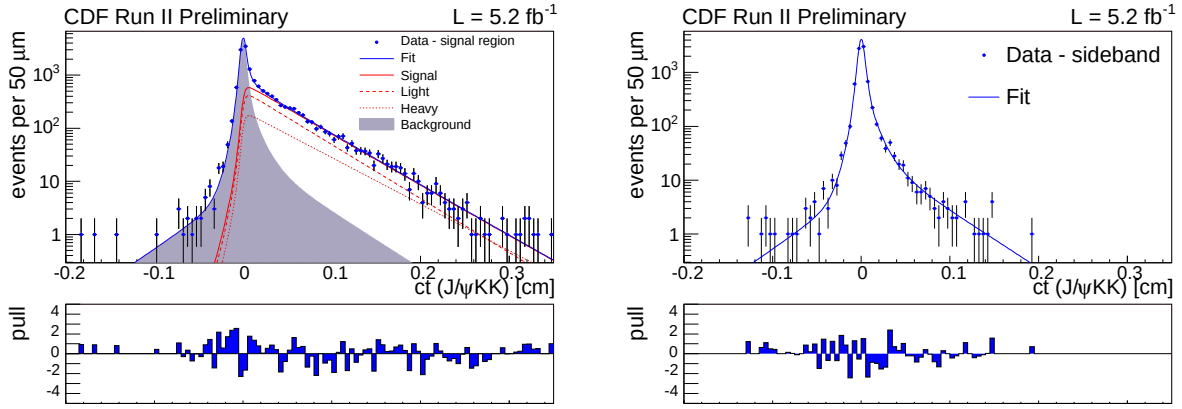


FIG. 7: $B_s^0$ $ct$ likelihood fit projections for the signal region (left) and sideband region (right).

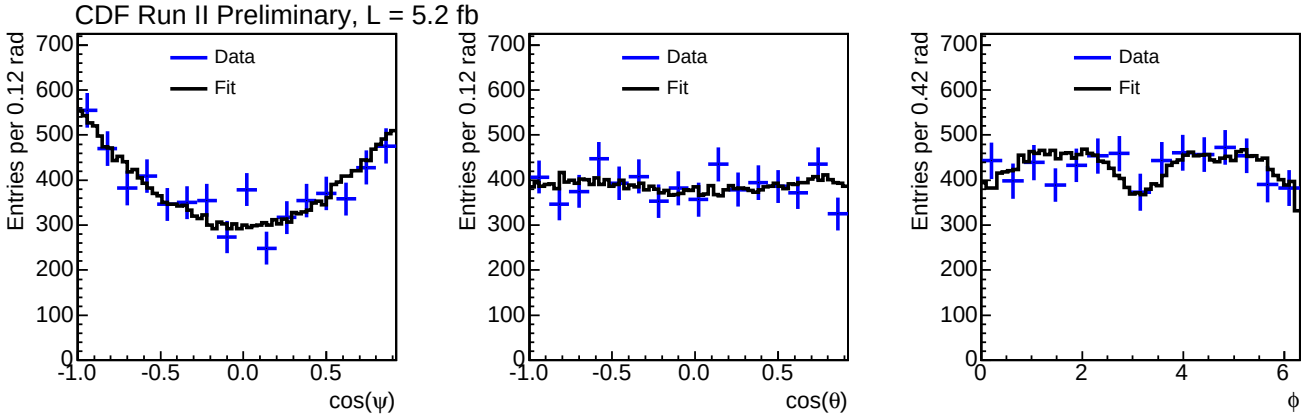


FIG. 8: Transversity angle projections of the sideband-subtracted signal for $\cos\psi_T$ (left), $\cos\theta_T$ (center), and $\phi_T$ (right).

To obtain the final confidence contours, we calculate p-values for grid of points in the $\beta_s$-$\Delta\Gamma$ plane. We use a likelihood ratio, defined as the ratio of the value of the likelihood in which $\beta_s^{J/\psi\phi}$ and $\Delta\Gamma$ are fixed in the fit to values of $\beta_s^{J/\psi\phi} = 0.02$ and $\Delta\Gamma = 0.096$ ps$^{-1}$ relative to the value of the likelihood in which $\beta_s^{J/\psi\phi}$ and $\Delta\Gamma$ float freely in the fit, to determine the p-value. We simulate 1000 experiments using input parameters same as we extract in fit to data and compare obtained distribution of likelihood ratio to value from data. In addition, we generate set of additional sixteen "alternate universes" in which the nominal values of all nuisance parameters have been varied randomly by $\pm 5\sigma$ around values obtain in data. We then choose the most conservative adjustment and p-value for the final result. The adjustment curves for the 2D profile likelihood and the final, adjusted two-dimensional confidence regions in $\beta_s^{J/\psi\phi} - \Delta\Gamma$ plane are shown in Fig. 9. We find that the p-value at the standard model expectation is 44%.

We have also determined the one-dimensional profile likelihood for $\beta_s^{J/\psi\phi}$. This result is also adjusted based on a one-dimensional mapping calculated from p-values at the standard model point $\beta_s^{J/\psi\phi} = 0.02$ using 1,000 default pseudo-experiments and 1,000 pseudo-experiments in each of sixteen "alternate universes". The adjustment curves for the one-dimensional profile likelihood and the final adjusted profiles are shown in Fig. 10. The final one-dimensional

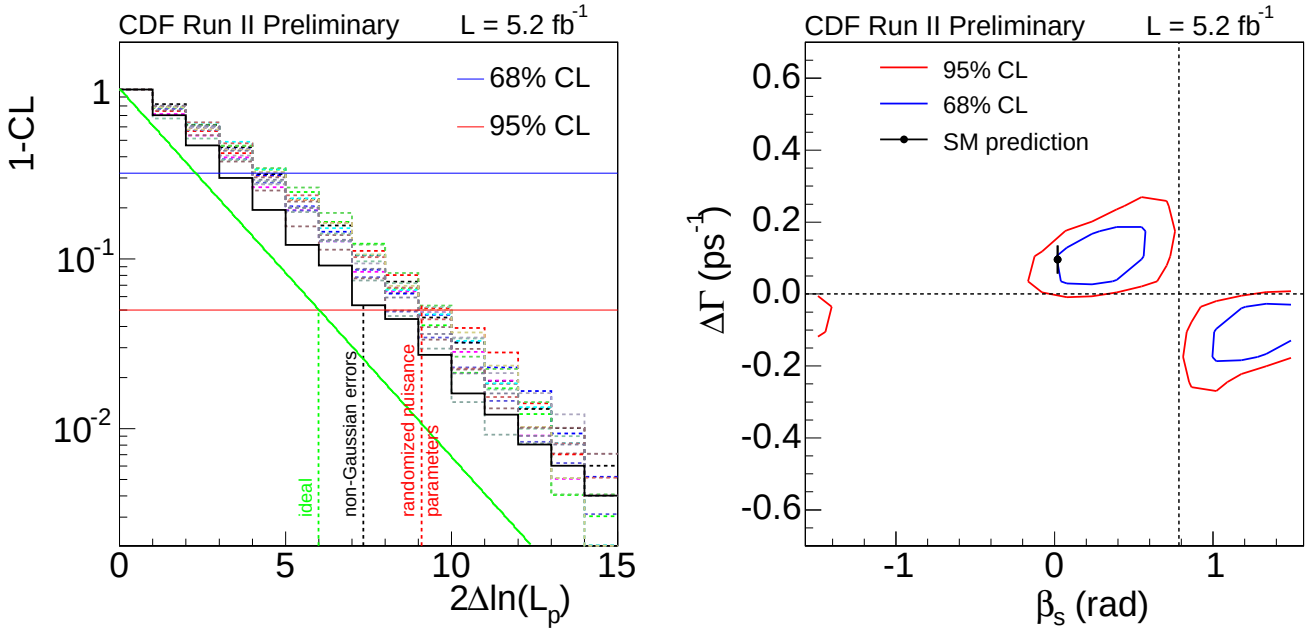


FIG. 9: Cumulative likelihood ratio distribution for the two-dimensional profile likelihood (left) with the likelihood ratios for all of the "alternate universes" (colored histograms) overlaid on that from the "default" universe (black histogram). Adjusted two-dimensional profile likelihood of $\beta_s^{J/\psi\phi}$ and $\Delta\Gamma$ in 5.2 fb$^{-1}$ of data (right). The standard model point is indicated by the black point with error bars. The p-value at the standard model point is 44%.

ranges are

$$\begin{aligned}\beta_s^{J/\psi\phi} &\in [0.02, 0.52] \cup [1.08, 1.55] \text{ at } 68\%\text{C.L,}\\ \beta_s^{J/\psi\phi} &\in [-\pi/2, -1.44] \cup [-0.13, 0.68] \cup [0.89, \pi/2] \text{ at } 95\%\text{C.L.}\end{aligned}$$

The p-value at the standard model point is 31%.

In addition to the flavor-tagged 2D and 1D results, we also quote a 2D coverage-adjusted contour in the $\beta_s^{J/\psi\phi} - \Delta\Gamma$ plane for the likelihood fit without flavor tagging, shown in Figs. 11. The coverage adjustment in the untagged case is completely analogous to the adjustments made in the other cases, with 1,000 pseudo-experiments generated at the standard model point in both the "default" universe and in sixteen "alternate" ones. The p-value at the standard model point for the untagged contour is 8%. As in the case of the flavor-tagged contours, the untagged contour includes any possible contribution from S-wave states to the $\phi$ mass window.

## VI. CROSS-CHECKS OF LIKELIHOOD CONTOURS

### A. Effect of coverage adjustment

The effect of the coverage adjustment on the one and two-dimensional contours can be seen in Fig. 12, which shows the unadjusted profile likelihoods. This difference is expected to decrease as statistics becomes high enough that the errors a Gaussian regime and the nuisance parameters are better constrained.

### B. Time-dependence of result

In order to check for possible time-dependence of the result, we have divided the data in three approximately equal periods of data-taking: 0 - 1.35 fb$^{-1}$, 1.35 - 2.8 fb$^{-1}$, and 2.8 - 5.2 fb$^{-1}$. The unadjusted contours for the three independent datasets are shown in Fig. 13. The variations observed are consistent with those seen in pseudo-experiments of similar size [15].

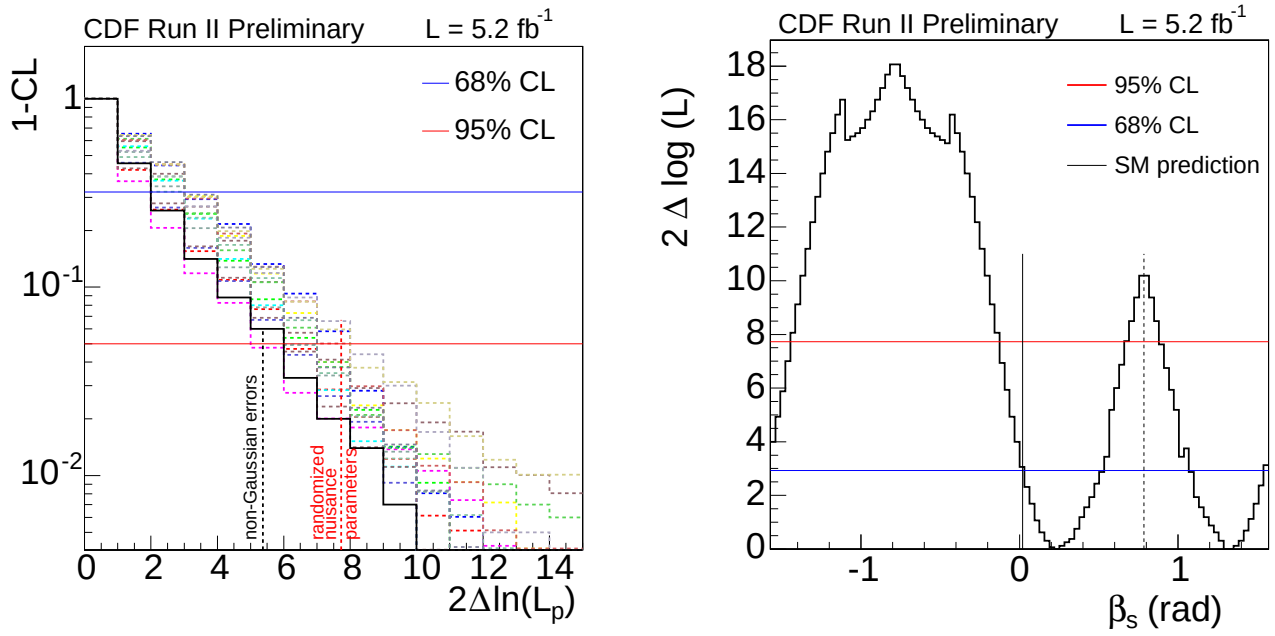


FIG. 10: Cumulative likelihood ratio distribution for the one-dimensional profile likelihood (left) with the likelihood ratios for all of the "alternate universes" (colored histograms) overlaid on that from the "default" universe (black histogram). Coverage-adjusted one-dimensional profile likelihood for $\beta_s^{J/\psi\phi}$ in 5.2 fb$^{-1}$ of data (right). The p-value at the standard model point is 31%.

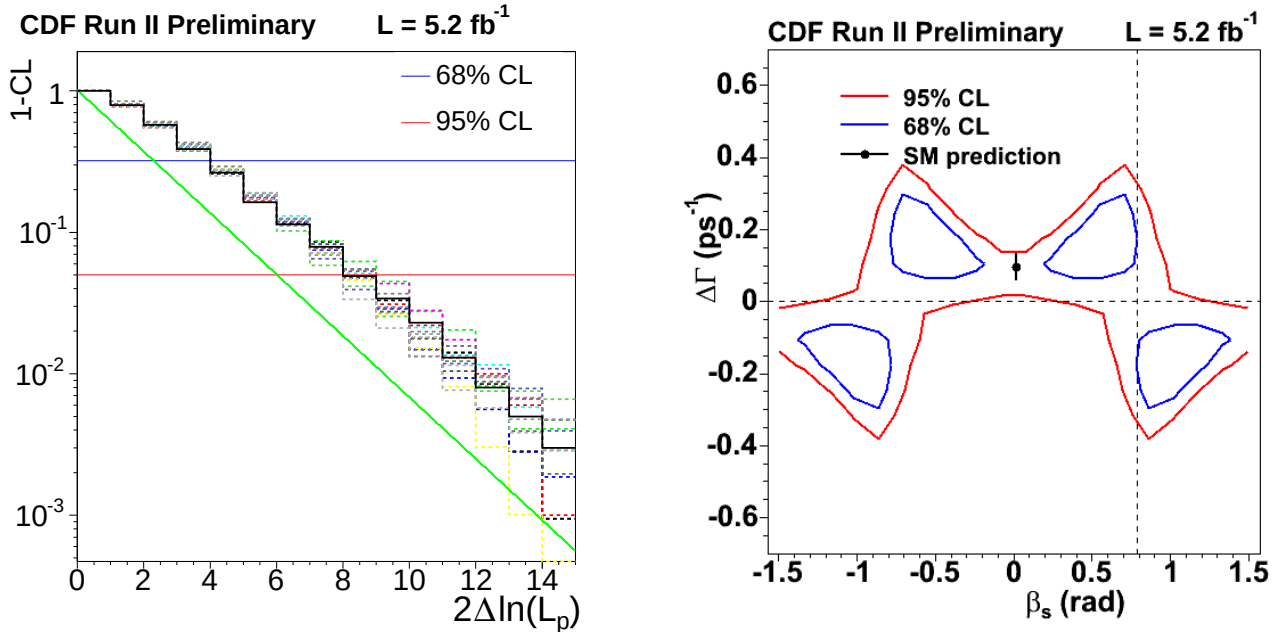


FIG. 11: Cumulative likelihood ratio distribution for the untagged profile likelihood (left) with likelihood ratios for all of the "alternate universes" (colored histograms) overlaid on that from the "default" universe (black histogram). Coverage-adjusted, untagged two-dimensional profile likelihood of $\beta_s^{J/\psi\phi}$ and $\Delta\Gamma$ in 5.2 fb$^{-1}$ of data (left). The standard model point is indicated by the black point with error bars. The p-value at the standard model point is 8%.

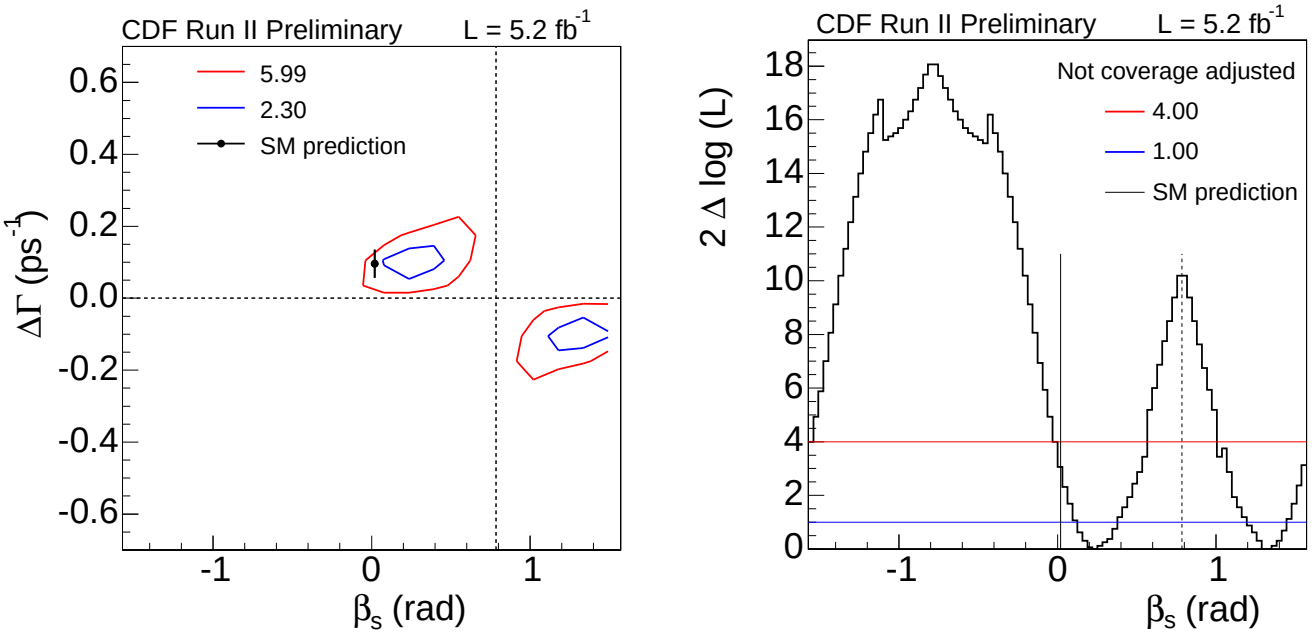


FIG. 12: Tagged two-dimensional (left) and one-dimensional (right) profile likelihoods, unadjusted for non-Gaussian errors or variation of nuisance parameters.

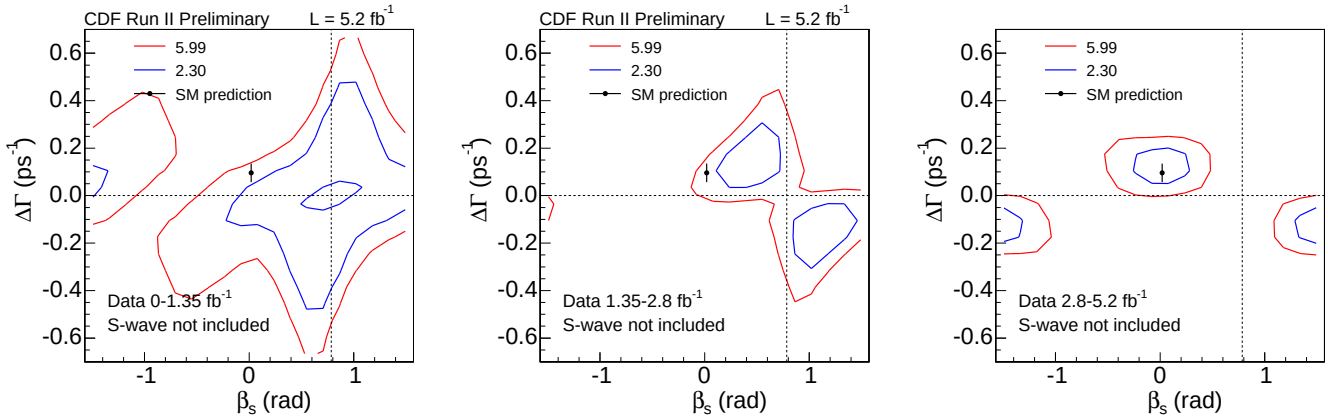


FIG. 13: Tagged two-dimensional profile likelihoods, unadjusted for non-Gaussian errors or variation of nuisance parameters, in the first 1.35 fb$^{-1}$ of data used in the measurement (left), the middle 1.35 - 2.8 fb$^{-1}$ data used (center), and the last 2.8 - 5.2 fb$^{-1}$ data used (right).

### C. *S*-wave contribution to likelihood fit

The fraction of $S$-wave observed in the likelihood fit is $< 6.7\%$ at the 95 % confidence level, shown in the left plot of Fig. 14, for $m(K^+K^-) \in [1.009, 1.028]$ GeV/$c^2$. We have cross-checked the $S$-wave contamination in the $K^+K^-$ invariant mass distribution and find results consistent with a null contribution, as can be seen in the right plot of Fig. 14, although uncertainty on the fitted $S$-wave fraction is on the order of a few percent. As a cross-check, we have overlaid the default 2D contour, with no coverage adjustment, with a contour obtained without an $S$-wave contribution in Fig. 15. The effect of adding the $S$-wave is negligible, due to the small fraction observed in the fit.

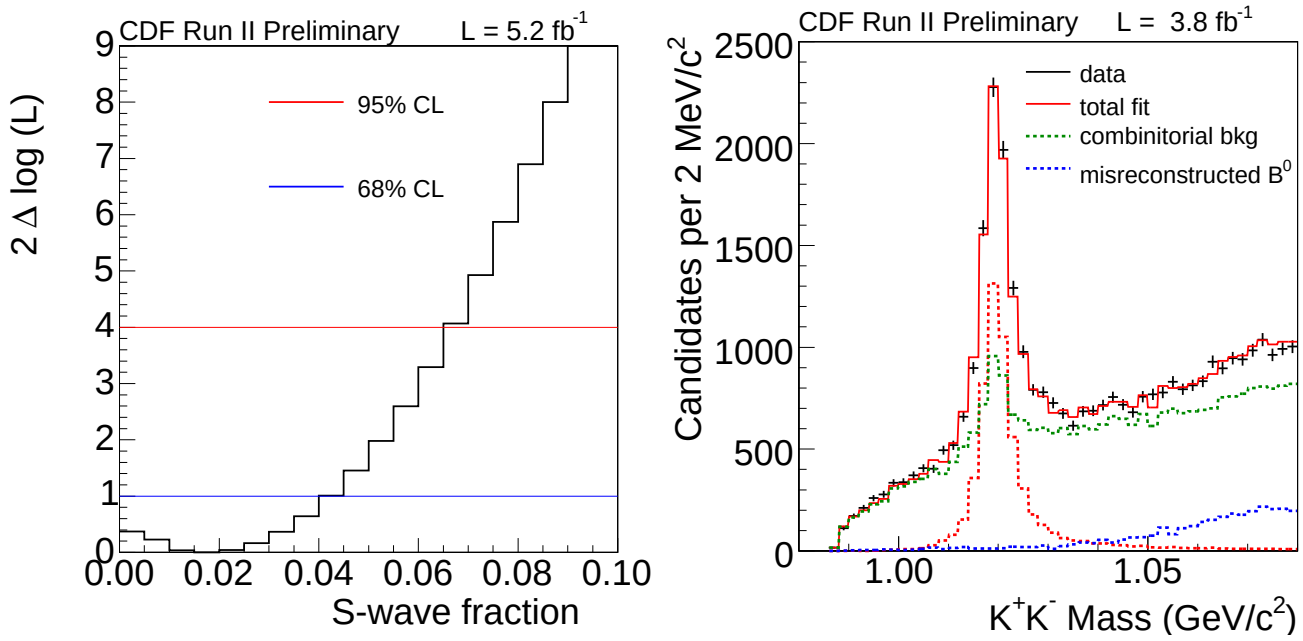


FIG. 14: $S$-wave fraction observed in the maximum likelihood fit in the invariant mass window $m(K^+K^-) \in [1.009, 1.028]$ GeV/$c^2$ (left). Invariant mass of $K^+K^-$ system without an $S$-wave contribution included.

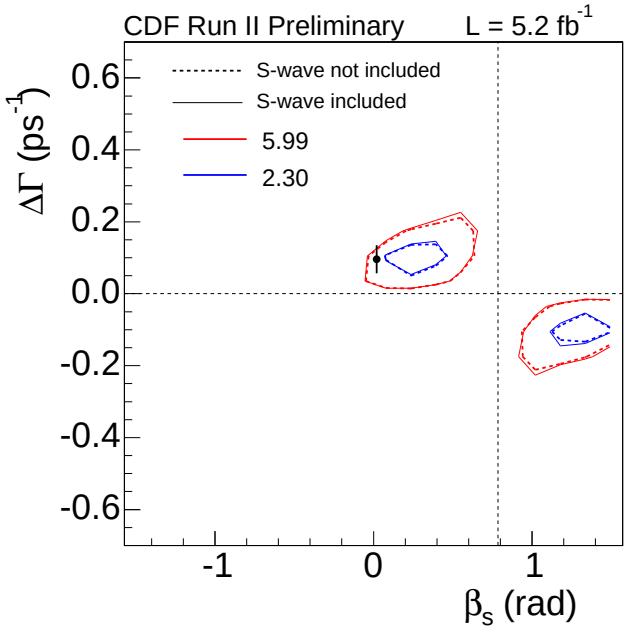


FIG. 15: Comparison of unadjusted $\beta_s^{J/\psi\phi} - \Delta\Gamma$ profile likelihoods with and without an $S$-wave contribution.

## VII. LIKELIHOOD FIT WITH STANDARD MODEL CONSTRAINTS

We also measure the inverse of the mean decay width $\tau_s$, the decay width difference $\Delta\Gamma$, the transversity amplitudes $|A_0(0)|^2$ and $|A_\parallel(0)|^2$ (where $|A_\perp(0)|^2 \equiv 1 - |A_0(0)|^2 - |A_\parallel(0)|^2$), and the strong phase $\delta_\perp$ with the standard model constraint that $\beta_s^{J/\psi\phi} = 0.0$. Previously, point estimates have only been possible in the likelihood fit without flavor tagging [2, 16]. However, with 5.2 fb$^{-1}$ of data we now have enough statistics to reliably use the flavor-tagged fit to determine point estimates for the above-mentioned quantities. We are still unable to reliably determine a point estimate for the strong phase $\delta_\parallel$, as it's central value is near $\pi$, which is a symmetric point in the likelihood. Consequently, the errors returned by the likelihood fit are unreliable.

We assign systematic uncertainties from studies in which we generate systematic variations of our default pseudo-experiments, which correspond to our default fit model, and then fit as we normally would. We also produce a set of reference pseudo-experiments with no systematic variations, and fit these in the same way. For each systematic effect, we quote the associated error as the difference between the mean shift from the input value for the pseudo-experiments with and without the systematic effect generated. We run 1000 pseudo-experiments for each systematic effect and for the reference model, using the same seed for randomization in each case in order to minimize any statistical fluctuations.

The systematic effects that we include are described below. The modeling of the background lifetime is the most significant source of systematic uncertainties in the determination of both $\Delta\Gamma$ and the lifetime, while the transversity amplitudes are primarily affected by the knowledge of the signal angular efficiencies. The systematic uncertainties assigned are listed in Table II.

- Signal angular efficiency

  In order to determine the systematic uncertainty due to the modeling of the signal angular efficiencies, we generate pseudo-experiments with the angular efficiencies taken from 3D histograms of realistic Monte Carlo that take into account detector effects and fit them with our default fit which parameterizes the efficiencies by spherical harmonics and Legendre polynomials. We study the effect of both re-weighted and non-reweighted Monte Carlo in two separate studies. These systematic uncertainties are then added in quadrature to be included in the final systematics table. The study using non-reweighted Monte Carlo as inputs allows us to test any effect introduced by the Monte Carlo re-weighting.

- Signal mass model

  By default we fit the signal $B_s^0$ mass with a single Gaussian model. To analyze the effect of a potential mis-modeling, we generate pseudo-experiments with a double Gaussian model and two mass error scale factors and fit these with the default fit. We get the parameters for generating the pseudo-experiments by fitting the data with two Gaussians and two mass error scale factors.

- Background mass model

  By default we fit the background mass distribution with a first order polynomial. To analyze the effect of a potential mis-modeling, we generate pseudo-experiments with a 2nd order polynomial distribution with the coefficients taken from a 2nd order polynomial fit to the data background. These are fitted with the default fit to test the systematic effect of potentially mis-modeling the background mass distribution.

- Lifetime resolution model

  In order to assess the systematic uncertainty due to the modeling of the lifetime resolution, we generate pseudo-experiments with an alternate model to the two scale factor, double Gaussian resolution model used in the default fit. The alternate model used to test the systematic uncertainty consists of three Gaussians with three separate scale factors, two of which correspond to those fitted in data and the third which is a value between those. It should be noted that we do not bin the lifetime resolution in $\sigma c\tau$.

- Background lifetime fit model

  The systematic uncertainty due to our background lifetime model is assessed by generating pseudo-experiments with background lifetimes taken from a histogram of the lifetime distribution for the sidebands of the $B_s^0$ mass peak in data and fitting them with the default fit.

- Angular background model and correlations

  We also investigate correlations that have been observed in the background angles, specifically a correlation between the background angular distributions and the error on the lifetime, and a non-factorization between the angles $\phi$ and $cos(\theta)$. For the correlation between background angles and $\sigma(c\tau)$, we generate toys using as input

background angles histograms in three bins of $\sigma(c\tau)$. To assess the systematic effect of the non-factorization of $\phi$ and $cos(\theta)$, we generate toys with $cos(\theta)$ and $cos(\psi)$ sampled from background angular distributions taken from the data sidebands, and $\phi$ sampled according to the generated $cos(\theta)$ value from one of three histograms in different $cos(\theta)$ bins. We use these distributions to generate pseudo-experiments and then fit with our default background angular distribution to estimate the systematic error from our background angular model.

- $B^0$ cross-feed

  In order to account for systematic uncertainties due to $B^0 \to J/\psi\, K^{*0}$ events mis-reconstructed as $B_s^0 \to J/\psi\, \phi$, in which the pion from the $K^{*0} \to K^+\pi^-$ decay is mis-identified as a kaon, we generate pseudo-experiments with 2.2% of the signal events coming $B^0 \to J/\psi\, K^{*0}$ decays. The fraction of potential cross-feed events is calculated by analyzing the relative proportion of Monte Carlo $B^0 \to J/\psi\, K^{*0}$ events reconstructed as $B_s^0 \to J/\psi\, \phi$ that pass our neural network selection cuts compared to real $B_s^0 \to J/\psi\, \phi$ events. The pseudo-experiments we generate are fitted with the default model, which does not include a $B^0$ cross-feed element.

- SVX alignment

  The measurement of $\beta_s^{J/\psi\phi}$ is affected by the alignment of the SVX through the contribution of the mixing frequency $\Delta m_s$ which is sensitive to the length scale of the SVX. We follow the principals of the previous update and include a 2 $\mu$m systematic uncertainty on the lifetime, and find the effect on the other parameters by generating pseudo-experiments with a shift of $\pm 2$ $\mu$m to the measured lifetime and the other input parameters unaltered, then fitting with the default fit.

- Mass error distribution

  In the default likelihood function, we assume that the mass error distribution is the same for signal and sideband events. In the $B \to J/\psi X$ lifetimes analysis [17], it was found that differences in the signal and background distributions could have a systematic effect on the $B$ lifetime. We check this effect in our fitter by generating pseudo-experiments with mass error distributions taken from the sideband and sideband-subtracted data separately and fitted with the default assumption. The systematic error on the lifetime found in this study, 0.8 $\mu$m agrees very well with the 0.9 $\mu$m effect seen in Ref. [17].

- $c\tau$ error distribution

  We may introduce a systematic effect through the modeling of $\sigma_{c\tau}$. We use a "Punzi" parametrization [18] to model the lifetime error in signal and background separately in the default fit, with the coefficients taken from a fit to data. To test the effect of any mis-modeling due to this parametrization, we generate pseudo-experiments with $\sigma c\tau$ randomly sampled from data histograms of sideband and sideband subtracted data. It was observed in Ref. [17] that there was a very small effect arising from $\sigma(c\tau) - mass$ correlations in the $B \to J/\psi X$ lifetime measurement. We account for such a potential effect in this systematic study by taking the $c\tau$ error distributions from the upper and lower sidebands separately according where the mass of background events lie.

- Pull bias

  Slight biases are observed in pseudo-experiments generated with the default parameters obtained on fits to data for some of the quantities. We include these biases as systematic uncertainties.

Including the above systematic uncertainties in our point estimates assuming the standard model, we find

$$\begin{aligned} c\tau_s &= 458.6 \pm 7.6\ (\text{stat.}) \pm 3.6\ (\text{syst.})\ \mu\text{m} \\ \Delta\Gamma &= 0.075 \pm 0.035\ (\text{stat.}) \pm 0.01\ (\text{syst.})\ ps^{-1} \\ |A_\parallel(0)|^2 &= 0.231 \pm 0.014\ (\text{stat}) \pm 0.015\ (\text{syst.}) \\ |A_0(0)|^2 &= 0.524 \pm 0.013\ (\text{stat}) \pm 0.015\ (\text{syst.}) \\ \delta_\perp &= 2.95 \pm 0.64\ (\text{stat}) \pm 0.07\ (\text{syst.}) \end{aligned} \tag{23}$$

which are consistent with previous determinations of these quantities [2, 16]. The measured $B_s^0$ lifetime is the most precise to-date, as are the measurements of $\Delta\Gamma$ and the transversity amplitudes [2, 19, 20].

## VIII. CONCLUSIONS

We present an updated measurement of the $B_s$ mixing phase $\beta_s$ on the dataset corresponding to an integrated luminosity of 5.2 fb$^{-1}$. Although the discrepancy with the standard model has decreased from the previous iteration

| Systematic | $\Delta\Gamma$ [ps$^{-1}$] | $c\tau_s$ [ps] | $\lvert A_\parallel(0)\rvert^2$ | $\lvert A_0(0)\rvert^2$ | $\delta_\perp$ |
|---|---|---|---|---|---|
| Signal efficiency | | | | | |
| Parameterization | 0.0024 | 0.96 | 0.0076 | 0.008 | 0.016 |
| MC re-weighting | 0.0008 | 0.94 | 0.0129 | 0.0129 | 0.022 |
| Signal mass model | 0.0013 | 0.26 | 0.0009 | 0.0011 | 0.009 |
| Background mass model | 0.0009 | 1.4 | 0.0004 | 0.0005 | 0.004 |
| Resolution model | 0.0004 | 0.69 | 0.0002 | 0.0003 | 0.022 |
| Background lifetime model | 0.0036 | 2.0 | 0.0007 | 0.0011 | 0.058 |
| Background angular distribution: | | | | | |
| Parameterization | 0.0002 | 0.02 | 0.0001 | 0.0001 | 0.001 |
| $\sigma(c\tau)$ correlation | 0.0002 | 0.14 | 0.0007 | 0.0007 | 0.006 |
| Non-factorization | 0.0001 | 0.06 | 0.0004 | 0.0004 | 0.003 |
| $B^0 \to J/\psi K^*$ cross-feed | 0.0014 | 0.24 | 0.0007 | 0.0010 | 0.006 |
| SVX alignment | 0.0006 | 2.0 | 0.0001 | 0.0002 | 0.002 |
| Mass error | 0.0001 | 0.58 | 0.0004 | 0.0004 | 0.002 |
| c$\tau$ error | 0.0012 | 0.17 | 0.0005 | 0.0007 | 0.013 |
| Pull bias | 0.0028 | | 0.0013 | 0.0021 | |
| **Totals** | 0.01 | 3.6 | 0.015 | 0.015 | 0.07 |

TABLE II: Summary of systematic uncertainties assigned.

from a 1.8 $\sigma$ discrepancy to an $\approx 1$ $\sigma$ discrepancy, the result is now in better agreement with the values of $\Delta\Gamma$ and $\beta_s^{J/\psi\phi}$ expected from models of new physics, in which $|\Gamma_{12}|$ does not receive significant contribution from new physics, and with the result obtained by the D0 collaboration in their most recent measurement of the same quantities [3]. The uncertainty on $\Delta\Gamma$ is now comparable to the theoretical uncertainty, making the 1D profile likelihood in $\beta_s^{J/\psi\phi}$ more physically interesting. The point estimates obtained assuming a standard model value of $\beta_s^{J/\psi\phi}$ provide some of the most precise estimates of these quantities.


[1] T. Aaltonen et al. (CDF Collaboration), Phys. Rev. Lett. **100**, 161802 (2008).
[2] http://www-cdf.fnal.gov/physics/new/bottom/080724.blessed-tagged_BsJPsiPhi_update_prelim/.
[3] http://www-d0.fnal.gov/Run2Physics/WWW/results/prelim/B/B58/.
[4] S. Stone and L. Zhang, Phys. Rev. D **79**, 074024 (2009).
[5] Y. Xie, P. Clarke, G. Cowan, and F. Muheim, JHEP **09**, 074 (2009).
[6] http://www-cdf.fnal.gov/physics/new/bottom/100204.blessed-sskt-calibration/index.html.
[7] D. Acosta et al. (CDF Collaboration), Phys. Rev. D **71**, 032001 (2005).
[8] G. Giurgiu, Ph.D. thesis, Carnegie Mellon Univ., FERMILAB-THESIS-2005-41 (2005).
[9] W. M. Yao et al. (Particle Data Group), J. Phys. G **33**, 1 (2006).
[10] A. S. Dighe, I. Dunietz, and R. Fleischer, Eur. Phys. J. C **6**, 647 (1999).
[11] M. Feindt (2004), arXiv:physics/0402093.
[12] T. Aaltonen et al. (CDF Collaboration), Phys. Rev. D **77**, 072003 (2008).
[13] CDF Collaboration, CDF note 8206, http://www-cdf.fnal.gov/physics/new/bottom/060302.blessed-sskt/.
[14] A. Abulencia et al. (CDF Collaboration), Phys. Rev. Lett. **97**, 242003 (2006), and references therein.
[15] http://theory.fnal.gov/jetp/talks/ggiurgiu_wine_and_cheese_beta_s.pdf.
[16] T. Aaltonen et al. (CDF Collaboration), Phys. Rev. Lett. **100**, 121803 (2008).
[17] http://www-cdf.fnal.gov/physics/new/bottom/091217.blessed-JpsiX4.3/jpsix.html.
[18] G. Punzi (2004), arXiv:physics/0401045.
[19] V. M. Abazov et al. (D0 Collaboration), Phys. Rev. Lett. **102**, 032001 (2009).
[20] http://www.slac.stanford.edu/xorg/hfag/.